



# Precipitation synthesis of $\text{WO}_3$ for $\text{NO}_x$ removal using PEG as template

E. Luévano-Hipólito<sup>a</sup>, A. Martínez-de la Cruz<sup>a,\*</sup>, Q.L. Yu<sup>b</sup>, H.J.H. Brouwers<sup>b</sup>

<sup>a</sup>CIIDIT, Facultad de Ingeniería Mecánica y Eléctrica, Universidad Autónoma de Nuevo León, Ciudad Universitaria, C.P. 66451, San Nicolás de los Garza, N. L., México

<sup>b</sup>Unit of Building Physics and Services, Department of the Built Environment, Eindhoven University of Technology, P.O. Box 513, 5600 MB Eindhoven, The Netherlands

Received 18 February 2014; received in revised form 9 April 2014; accepted 9 April 2014  
Available online 19 April 2014

## Abstract

$\text{WO}_3$  polyhedral particles were prepared by precipitation using polyethylene glycol (PEG) as template and steric stabilizer. The growth and aggregation degree of  $\text{WO}_3$  polyhedral particles were affected by the thermal treatment, which caused different physical properties in the final product. The samples were characterized by X-ray powder diffraction (XRD), scanning electron microscopy (SEM), UV–vis diffuse reflectance spectroscopy (UV–vis DRS) and adsorption–desorption  $\text{N}_2$  isotherms (BET).  $\text{WO}_3$  samples were tested as photocatalysts in the oxidation reaction of nitric oxide (NO) under UV irradiation. The photocatalytic activity of the samples was associated with its morphology and their surface area values. The present work demonstrates that polyhedral particles of  $\text{WO}_3$  are effective photocatalytic functional materials for air purification by elimination of NO.

© 2014 Elsevier Ltd and Techna Group S.r.l. All rights reserved.

**Keywords:** Heterogeneous photocatalysis;  $\text{WO}_3$ ; Polyethylene glycol; NO;  $\text{NO}_x$

## 1. Introduction

The generic term  $\text{NO}_x$  refers to a group of oxides formed by the chemical combination of nitrogen and oxygen in different ratios ( $\text{NO} + \text{NO}_2$ ) and constitutes one of the most common air pollutants. Among the various proposed technologies to solve this problem, the heterogeneous photocatalysis has received an increasing interest in recent years [1–6]. The reactions involved in heterogeneous photocatalysis are highly attractive because they take place at room temperature and usually, the photocatalyst can be used almost indefinitely. Several semiconductor oxides have been proposed as photocatalysts, in particular  $\text{WO}_3$  oxide has attractive properties such as a small energy band gap (2.5–2.8 eV), and a high oxidation power of their photogenerated holes ( $+3.1V_{\text{NHE}}$ ) which are capable to oxidize  $\text{H}_2\text{O}$  to  $\text{O}_2$  [7,8]. Several methods have been developed to synthesize  $\text{WO}_3$  in order to improve their textural properties, and consequently increase the photocatalytic activity [9–11].

The precipitation of ammonium tungstate hydrate in acid medium is the most common preparation method to synthesize  $\text{WO}_3$  [11,12]. However, the lack of a stabilizer in the reaction medium promotes the formation of large agglomerates resulting in samples with low photocatalytic activity. The formation of big agglomerates reduces the surface area value of  $\text{WO}_3$  due to an unavoidable sintering process which consists of the pore collapse during the calcination to complete the formation of oxide. For this reason, one strategy to increase the surface area of the oxide is to add a polymer to tungstate suspension, since the presence of the polymer promotes porosity in the sample after the calcination. In addition, the polymer chains in tungstate suspension act as steric stabilizer that prevents aggregation of particles. Currently, polyethylene glycol (PEG, in a variety of molecular weights) is considered as an effective steric stabilizer and template during the synthesis of  $\text{TiO}_2$  photocatalysts with high surface area values [13–15]. PEG is a water soluble organic polymer with a structure of  $\text{HO}-(\text{CH}_2-\text{O}-\text{CH}_2)_n-\text{OH}$ , where  $n$  represents the average number of oxyethylene groups. Besides the increase in the surface area, the PEG addition during synthesis plays an

\*Corresponding author.

E-mail address: [azael.martinezdl@uanl.edu.mx](mailto:azael.martinezdl@uanl.edu.mx) (A. Martínez-de la Cruz).

important role in the mechanism of formation of nanosized structures. In the present work,  $\text{WO}_3$  was prepared by a precipitation method assisted with a PEG polymer as template and a steric stabilizer. The oxidation of NO was employed as model reaction to evaluate the photocatalytic activity of  $\text{WO}_3$  samples obtained. The effect of the calcination time employed during synthesis of  $\text{WO}_3$  and the relative humidity (RH) of the air in the NO conversion reaction will be analyzed.

## 2. Experimental

### 2.1. Synthesis of $\text{WO}_3$

$\text{WO}_3$  photocatalysts were prepared by the precipitation method using PEG as template. In a typical synthesis, 0.0082 mol of ammonium tungstate hydrate ( $\text{H}_{42}\text{N}_{10}\text{O}_{42}\text{W}_{12} \cdot x\text{H}_2\text{O}$ ) (Aldrich, 99%) was dissolved in 20 mL of  $\text{HNO}_3$  solution (10% v/v) under continuous stirring. Subsequently, PEG was added into the tungstate solution to obtain a final concentration of 0.25 M. This process was accompanied with a vigorous stirring. After 1 h, the resulting suspension was maintained at 100 °C in a hot plate to promote the evaporation of the solvent. The resulting powders were heated at 500 °C for 4 h and 24 h to obtain polycrystalline powders. The obtained samples were labeled as WPC-*t* (WP0.25-4 and WP0.25-24), where *c* represents PEG concentration in the solution and *t* the calcination time used to obtain the polycrystalline powders. For comparative purpose, a sample of  $\text{WO}_3$  was obtained by precipitation of the oxide but in absence of PEG (WP0).

### 2.2. Characterization

The structural characterization was carried out by X-ray powder diffraction by using a Bruker D8 Advance diffractometer with Cu  $\text{K}\alpha$  radiation (40 kV, 30 mA). A typical run was made with a step size of 0.05° and a dwell time of 0.5 s. The morphology of the powders was analyzed by scanning electron microscopy by using a FEI Nova NanoSEM 200 with an accelerating voltage of 30 kV. The UV–vis diffuse reflectance absorption spectra of the samples were obtained in an Agilent Technologies UV–vis-NIR spectrophotometer model

Cary 5000 series equipped with an integrating sphere. The BET surface area measurements were carried out by adsorption–desorption  $\text{N}_2$  isotherms by means of a Bel-Japan Minisorp II surface area and pore size analyzer. The isotherms were evaluated at –196 °C after a pretreatment of samples at 150 °C for 24 h.

### 2.3. Photocatalytic experiments

The photocatalytic experiments were carried out in a homemade reactor designed in accordance with standard ISO 22197-1:2007 (Fig. 1). The experimental setup consisted of a planar reactor cell, an UVA light source, a chemiluminescent  $\text{NO}_x$  analyzer, and a gas supply. The main operating conditions of the system are summarized in Table 1. The samples for photocatalytic reactions were prepared by coating an aqueous suspension of the oxide on a glass substrate. The aqueous suspension was prepared by adjusting the mass to obtain 0.4 g of the photocatalyst on the substrate (dosage of 2 mg  $\text{cm}^{-2}$ ). Then, the suspension was coated onto the glass substrate by a brush. Subsequently the coated glass was dried at 100 °C in a

Table 1  
Experimental set-up main characteristics and operating conditions in the photocatalytic reactor.

Description	Operating conditions
Reactor	
Length (cm)	20
Width (cm)	10
Height (cm)	0.3
Volume ( $\text{cm}^3$ )	60
Substrate	
Length (cm)	20
Width (cm)	10
Light source	
Emission wavelength UV (nm)	300–400
Flow rate ( $\text{L min}^{-1}$ )	1
Irradiance flux ( $\text{W m}^{-2}$ )	10
Relative humidity (%)	10–50
$\text{NO}$ inlet concentration (ppm)	0.5

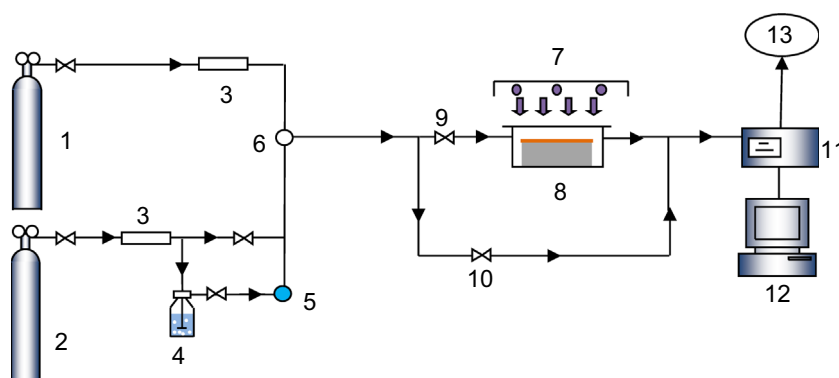


Fig. 1. Schematic diagram of the photocatalytic degradation set-up. 1. NO gas supply; 2. Synthetic air; 3. Mass controller meter; 4. Humidifier; 5. Humidity controller; 6. Temperature and relative humidity sensor; 7. Light source; 8. Reactor; 9. Valve; 10. Valve; 11.  $\text{NO}_x$  analyzer; 12. Computer; and 13. Vent.

hot plate to remove the water from the suspension. The resulting sample was calcinated at 500 °C for 4 h and 24 h for PEG removal. The NO concentration was monitored with a chemiluminescent NO<sub>x</sub> analyzer (HORIBA 370) with a sampling rate of 0.8 L min<sup>-1</sup>.

### 3. Results and discussion

#### 3.1. Characterization

The formation of the crystalline structure of WO<sub>3</sub> was followed by XRD. Fig. 2 shows XRD patterns of the prepared WO<sub>3</sub> powders by means of different experimental conditions. The diffraction lines of the WP0 and WP0.25-4 samples were readily indexed with the monoclinic structure of WO<sub>3</sub> in accord with the JCPDS Card no. 01-83-0950. The monoclinic structure still remains as the time of calcination was prolonged from 4 to 24 h (WP0.25-24). In addition, long calcination time promoted the formation of the hexagonal structure of WO<sub>3</sub> (JCPDS no. 01-85-2459) as can be seen in the sample WP0.25-24.

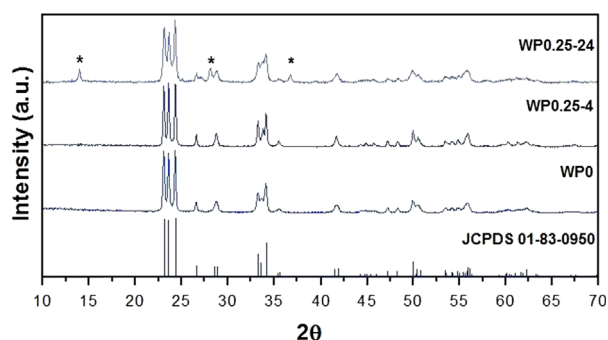


Fig. 2. XRD patterns of WO<sub>3</sub> samples prepared using PEG as template by precipitation method. (\*) WO<sub>3</sub> hexagonal.

The morphology of WO<sub>3</sub> was strongly dependent on the presence of PEG in the reaction medium, and on the calcination time as was revealed by SEM analyses. For example, the SEM image for the reference sample (WP0) showed a flake-like morphology with particle sizes higher than 350 nm (see Fig. 3a). On the contrary, the introduction of PEG into the reaction medium produced changes in the morphology of particles from a form of flakes to a polyhedral form as is shown in Fig. 3b and c. In addition, when the calcination time was extended to 24 h, the particle size of the polyhedral particles was higher in comparison with WP0.25-4. According to XRD results, hexagonal WO<sub>3</sub> appears in the sample WP0.25-24 (Fig. 3c). From the SEM results this evidence was not clear due to the homogeneity in the morphology of the particles and also possibly due to its low concentration in the sample.

Table 2 shows the BET surface area values of WO<sub>3</sub> samples prepared with PEG as template and different calcination times. When PEG was introduced into the reaction medium (WP0.25-4), the surface area increases from 2.9 to 7.1 m<sup>2</sup> g<sup>-1</sup>, which can be attributed to a decrease in the particle size of the oxide. On the other hand, the effect of calcination time in the BET surface area was also investigated. An increase in calcination time from 4 to 24 h leads to the decrease of the BET surface area from 7.1 to 4 m<sup>2</sup> g<sup>-1</sup> due to the agglomeration and growth of the polyhedral particles formed under these conditions (Fig. 3c). The decrease in the BET surface area also can be attributed to the presence of h-WO<sub>3</sub> in the samples, contrary to reports in the literature, in which the hexagonal structure has higher surface area than the monoclinic structure [16]. Fig. 4 shows the adsorption–desorption N<sub>2</sub> isotherms for the samples prepared under different experimental conditions. When PEG was introduced into the reaction medium, the isotherms obtained were categorized as type V with a hysteresis loop observed in the range of 0.6–1.0 P/P<sub>0</sub>, which is a

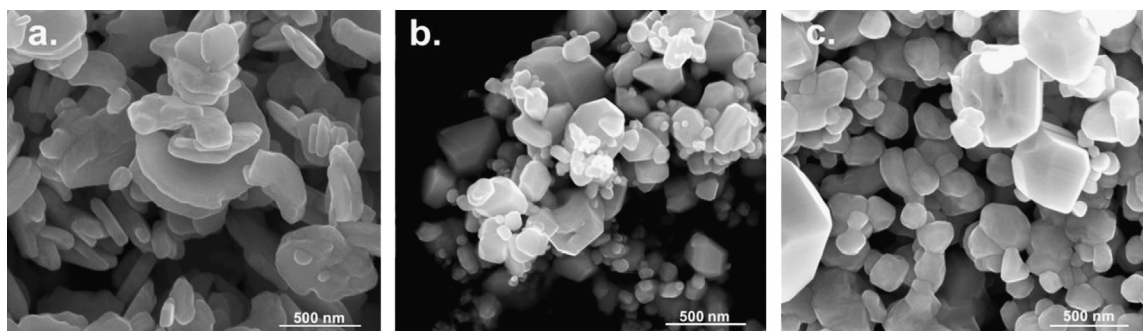


Fig. 3. SEM images of samples: a. WP0, b. WP0.25-4, and c. WP0.25-24.

Table 2  
Physical properties of the WO<sub>3</sub> samples prepared with PEG as template.

Sample	[PEG] (M)	<i>t</i> <sub>calcination</sub> (h)	Surface area BET (m <sup>2</sup> g <sup>-1</sup> )	Band gap (eV)	Particle size (nm)
WP0	0	24	2.9	2.6	350–400
WP0.25-4	0.25	4	7.1	2.4	200–250
WP0.25-24	0.25	24	4.0	2.5	250–300

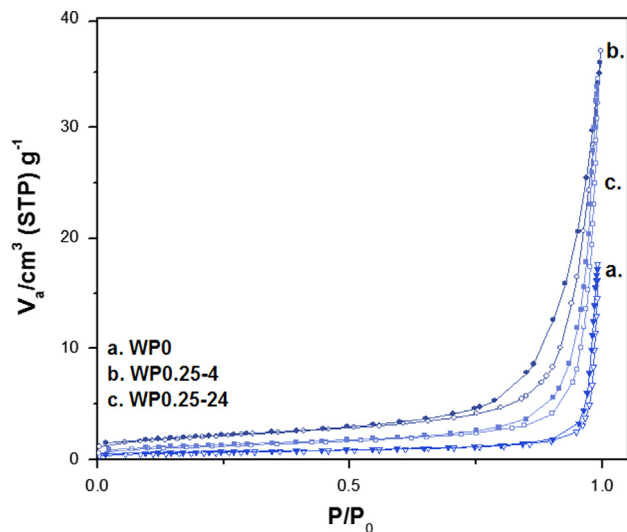


Fig. 4. Adsorption–desorption  $N_2$  isotherms of samples: a. WP0 ( $\nabla$ ), b. WP0.25-4 ( $\circ$ ), and c. WP0.25-24 ( $\square$ ). ( $\circ$ ) Adsorption and ( $\bullet$ ) desorption.

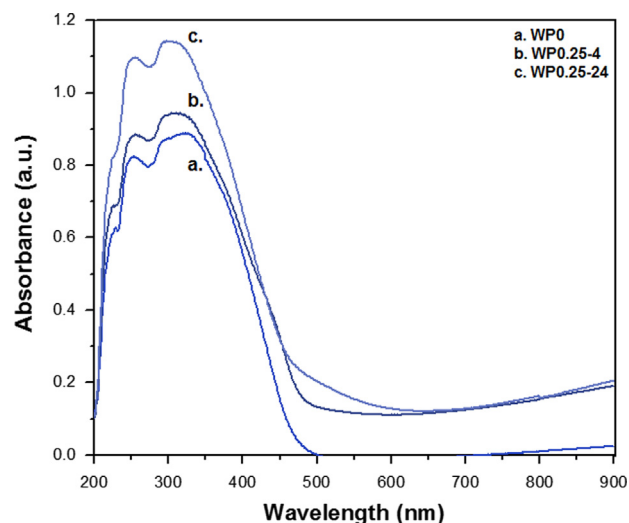


Fig. 5. Diffuse reflectance spectra of  $WO_3$  samples prepared using PEG as template by the precipitation method.

characteristic of mesoporous materials with low energy of adsorption [17]. The hysteresis loop was more pronounced for the sample WP0.25-4 due to its highest adsorption energy.

The diffuse reflectance of  $WO_3$  samples was analyzed by UV–vis spectroscopy. The absorption at 500 nm corresponds with the absorption edge of the material, and is due to an electronic transition from  $O_2^-$  to  $W^{6\pm}$  by charge transfer process from the valence band (mainly 2p orbitals of the oxygen anions) to the conduction band (mainly 5d orbitals of the tungsten cations) in  $WO_3$  [18]. It is important to note that WP0.25-24 shows a higher absorbance in comparison to WP0.25-4 and WP0. This can be attributed to the presence of h- $WO_3$  in this sample as impurity. From the data shown in Fig. 5, the energy band gap ( $E_g$ ) value of  $WO_3$  samples was calculated and listed in Table 2.

Fig. 6 shows a possible formation mechanism of  $WO_3$  particles prepared under different experimental conditions, according to the results discussed above. First, tungstate anion ( $H_2W_{12}O_{42}$ ) $^{10-}$  was produced when ammonium paratungstate was dissolved in an acid solution to finally form a precipitate of  $WO_3 \cdot H_2O$  particles [19]. Once the nucleation occurs, the PEG polymeric chain adsorbed on  $WO_3 \cdot H_2O$  surface inhibits the particle growth through a steric stabilization (WP0.25-4). When the calcination time increased from 4 to 24 h, the particles tend to form agglomerates in response to a decrease in its surface energy. In comparison, the SEM image of the reference sample (WP0) shows that  $WO_3$  particles can grow up and develop a flake-like morphology due to the lack of stabilizer during its formation. In this sense, PEG plays an important role as a steric stabilizer and as template leading to formation of polyhedral particles with smaller size than the material prepared from the reference method.

### 3.2. Photocatalytic activity

The photocatalytic activity of  $WO_3$  samples was evaluated by the removal of nitric oxide (NO) carried by a synthetic air under UVA light and 50% of relative humidity (RH). The NO concentration used was lower than that recommended by ISO 22197-1:2007, because 0.5 ppm is a concentration more

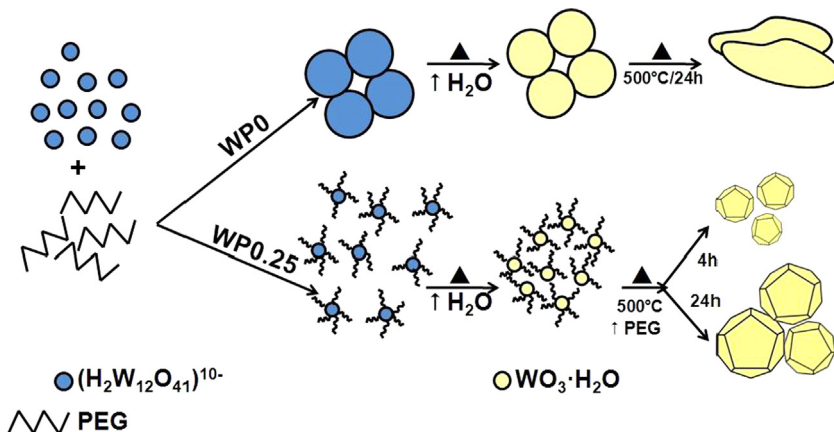


Fig. 6. Schematic explanation of the formation mechanism of  $WO_3$  particles prepared under different experimental conditions.

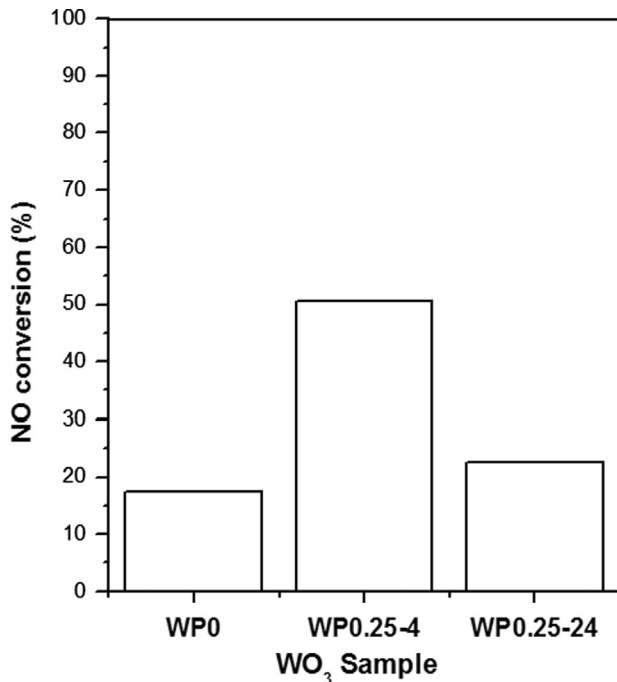


Fig. 7. NO conversion (%) using  $\text{WO}_3$  oxide prepared with PEG as template as photocatalyst. (UVA,  $\tau_R=3.6$  s,  $Q=1$  L/min $^{-1}$ ,  $E=10$  W/m $^{-2}$ ,  $RH=50\%$ ).

realistic in value than 1 ppm in environmental conditions. In Fig. 7, it can be seen that NO conversion (%) over the reference sample (WP0) is 17% in steady state under UVA radiation. Compared to this, the PEG introduction during the synthesis process has a significant enhancement in the photocatalytic activity of  $\text{WO}_3$  for the conversion of NO. In particular, this effect was more accentuated in the sample WP0.25-4 where NO conversion reached 50%. Nevertheless, the improvement in the photocatalytic activity of samples decreases as the time of calcination increases, as was shown for the sample WP0.25-24. This decrease in the photocatalytic activity can be attributed to the lower activity of the hexagonal phase present in the sample WP0.25-24 as was previously reported in the literature [16]. Previous studies have found that the hexagonal phase contains some cations as impurities in its channels, which are necessary to maintain hexagonal structure of  $\text{WO}_3$ . In this case, cation impurities can cause the decrease of the photocatalytic activity. Nevertheless, NO conversion degree (%) using  $\text{WO}_3$  prepared with PEG was always higher than that obtained with the reference sample (WP0). Fig. 8 shows the evolution of concentrations of NO,  $\text{NO}_2$ , and  $\text{NO}_x$  during the photocatalytic experiment using WP0.25-4 as photocatalyst. When the lamp was turned on and the reaction starts, NO concentration decreased quickly and reached a stable value of 50% of NO removed in about 20 min.  $\text{NO}_2$  concentration was increased as a product of the oxidation of NO to  $\text{NO}_2$  on  $\text{WO}_3$  surface.  $\text{NO}_x$  concentration ( $\text{NO}_x=\text{NO}+\text{NO}_2$ ) increased as NO concentration reached the steady state. If a complete oxidation of NO is assumed, the remaining gas was oxidized to nitrite or nitrate ions ( $\text{NO}_2^-/\text{NO}_3^-$ ) and fixed onto the surface of  $\text{WO}_3$  preventing more NO

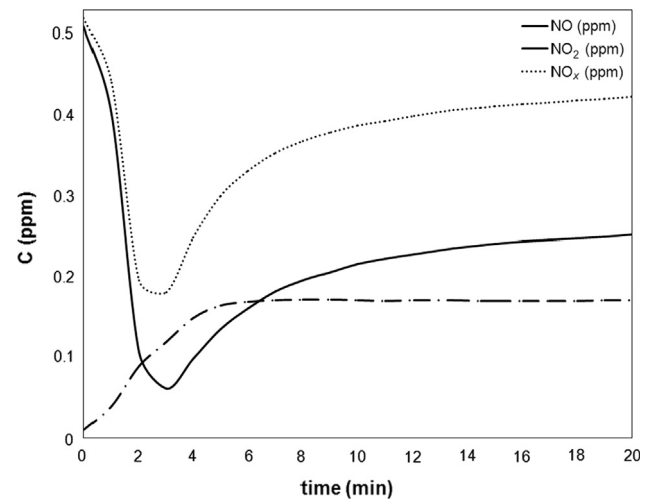


Fig. 8. Evolution of NO,  $\text{NO}_2$ , and  $\text{NO}_x$  concentrations during the course of their photocatalytic conversion.

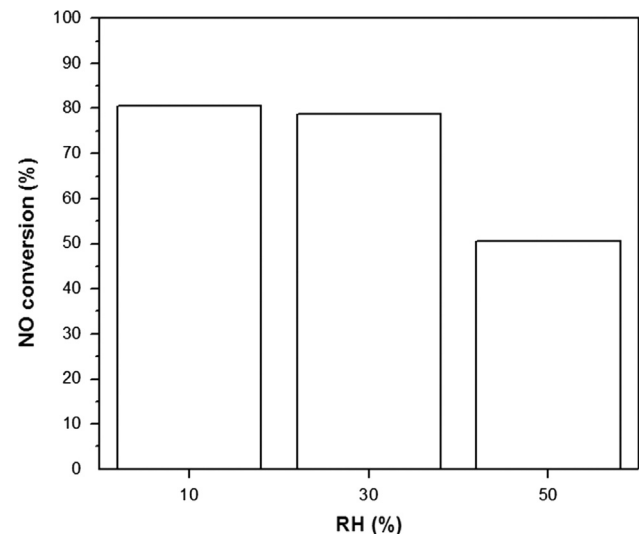


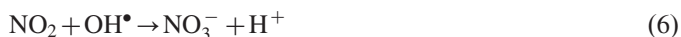
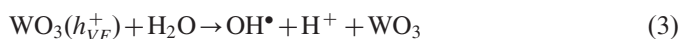
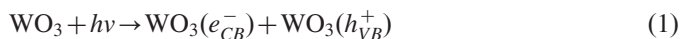
Fig. 9. NO conversion (%) using WP0.25-4 sample as photocatalyst with different relative humidities. (UVA,  $\tau_R=3.6$  s,  $Q=1$  L/min $^{-1}$ ).

molecules come into contact with the radicals generated during the photocatalytic process [20].

In addition, the photocatalytic activity was significantly affected by the relative humidity when WP0.25-4 was used as photocatalyst (see Fig. 9). The conversion of NO (%) was increased with the decrease in the relative humidity and achieved a maximum value of 80% with 10% RH. In the case of  $\text{NO}_x$  conversion, the experiment with 10% RH had the highest conversion in comparison with the values of 30% and 50% RH. When RH (%) was further increased, the conversion degree of NO decreased. The decrease in the photocatalytic activity was related with the competition between molecules of  $\text{H}_2\text{O}$  and NO for the active sites in  $\text{WO}_3$ , which produces a deactivation of the photocatalyst as was previously reported [21].

The photo oxidation reaction of NO when  $\text{WO}_3$  was used as photocatalyst can be explained by a mechanism involving the

oxidation of water to hydroxyl radical ( $\text{OH}^\bullet$ ) by photogenerated holes from the  $\text{WO}_3$  valence band. Then, the hydroxyl radicals react with NO to finally produces nitrite/nitrate ions ( $\text{NO}_2^-/\text{NO}_3^-$ ), which are innocuous molecules. The above is explained by Eqs. (1)–(6):



#### 4. Conclusions

$\text{WO}_3$  particles with polyhedral shape were successfully prepared by the precipitation method using PEG as template and steric stabilizer. The results from SEM images revealed that the morphology of  $\text{WO}_3$  was changed from flake to polyhedral shape when PEG was introduced into the reaction system. The calcination time for the preparation of samples also affected the morphology of particles leading to an unfavorable sintering process when the time went higher than 4 h. The synthesis of  $\text{WO}_3$  using 0.25 M of PEG concentration and 4 h of calcination time produced the material with the largest surface area.  $\text{WO}_3$  samples prepared using PEG during its formation showed higher photocatalytic activity than the reference sample. The sample with the highest surface area and lower calcination time (WP0.25-4) exhibited the highest photocatalytic activity which reached a 50% of conversion of NO in steady state. In comparison, the sample with monoclinic structure had a higher activity for this reaction than the sample with the hexagonal structure as was reported in the literature. NO conversion degree was strongly affected by the relative humidity due to the competition of adsorption sites between NO and  $\text{H}_2\text{O}$ . When 10% of RH was used in the system, the highest NO conversion degree was achieved (80%) with a global  $\text{NO}_x$  conversion probably until nitrite or nitrate ions ( $\text{NO}_2^-/\text{NO}_3^-$ ) during the photocatalytic process.

#### Acknowledgments

We wish to thank to the CONACYT for its invaluable support through the project 167018.

#### References

- [1] H. Ichiura, T. Kitaoka, H. Tanaka, Photocatalytic oxidation of  $\text{NO}_x$  using composite sheets containing  $\text{TiO}_2$  and a metal compound, *Chemosphere* 51 (2003) 855–860.

- [2] S. Matsuda, H. Hatano, Photocatalytic removal of  $\text{NO}_x$  in a circulating fluidized bed system, *Powder Technol.* 151 (2005) 61–67.
- [3] Q.L. Yu, H.J.H. Brouwers, Indoor air purification using heterogeneous photocatalytic oxidation. Part I: experimental study, *Appl. Catal. B* (2009) 454–461.
- [4] Q.L. Yu, H.J.H. Brouwers, Indoor air purification using heterogeneous photocatalysis. Part II: kinetic study, *Appl. Catal. B* 99 (2010) 58–65.
- [5] M.M. Ballari, H.J.H. Brouwers, Full scale demonstration of air-purifying pavement, *J. Hazard. Mater.* 254 (2013) 406–414.
- [6] E. Luévano-Hipólito, A. Martínez-de la Cruz, Q.L. Yu, H.J.H. Brouwers, Photocatalytic removal of nitric oxide by  $\text{Bi}_2\text{Mo}_3\text{O}_{12}$  prepared by co-precipitation method, *Appl. Catal. A* 468 (2013) 322–326.
- [7] G. Xin, W. Guo, T. Ma, Effect of annealing temperature on the photocatalytic activity of  $\text{WO}_3$  for  $\text{O}_2$  evolution, *Appl. Surf. Sci.* 256 (2009) 165–169.
- [8] G.R. Bramwenda, H. Arakawa, The visible light induced photocatalytic activity of tungsten trioxide powders, *Appl. Catal. A* 210 (2001) 181–191.
- [9] J. Sungpanich, T. Thongtem, S. Thongtem, Large-scale synthesis of  $\text{WO}_3$  nanoplates by a microwave-hydrothermal method, *Ceram. Int.* 38 (2012) 1051–1055.
- [10] D. Sánchez-Martínez, A. Martínez-de la Cruz, E. López Cuellar, Synthesis of  $\text{WO}_3$  nanoparticles by citric acid-assisted precipitation and evaluation of their photocatalytic properties, *Mater. Res. Bull.* 48 (2013) 691–697.
- [11] A. Martínez-de la Cruz, D. Sánchez M., E. López Cuellar, Synthesis and characterization of  $\text{WO}_3$  nanoparticles prepared by the precipitation method: evaluation of photocatalytic activity under vis-irradiation, *Solid State Sci.* 12 (2010) 88–94.
- [12] O. Nimitrakoolchai, S. Supothina, High-yield precipitation synthesis of tungsten oxide platelet particle and its ethylene gas-sensing, *Mater. Chem. Phys.* 112 (2008) 270–274.
- [13] K. Kato, A. Tsuzuki, Y. Torii, H. Taoda, T. Kato, Y. Butsugan, Morphology of thin anatase coatings prepared from alkoxide solutions containing organic polymer, affecting the photocatalytic decomposition of aqueous acetic acid, *J. Mater. Sci.* 30 (1995) 837–841.
- [14] K. Kajihara, T. Yao, Macroporous morphology of the titania films prepared by a sol-gel dip-coating method from the system containing poly(ethylene glycol). IV. General principle of morphology formation and effect of heat treatment, *J. Sol-Gel Sci. Technol.* 17 (2000) 173–184.
- [15] S. Bu, Z. Jin, X. Liu, L. Yang, Z. Cheng, Fabrication of  $\text{TiO}_2$  porous thin films using peg templates and chemistry of the process, *Mater. Chem. Phys.* 88 (2004) 273–279.
- [16] I.M. Szilágyi, B. Fórizs, O. Rosseler, A. Szegedi, P. Németh, P. Király, G. Tárkányi, B. Vajna, K. Varga-Josepovits, K. László, A.L. Tóth, P. Baranyai, M. Leskelä,  $\text{WO}_3$  photocatalysts: influence of structure and composition, *J. Catal.* 294 (2012) 119–127.
- [17] J.B. Condon, in: *Surface Area and Porosity Determinations by Physisorption*, Elsevier, Amsterdam, 2006, p. 8–9.
- [18] C. Martin, I. Martin, V. Rives, G. Solana, V. Loddó, L. Palmisano, A. Sclafani, Physicochemical characterization of  $\text{WO}_3/\text{ZrO}_2$  and  $\text{WO}_3/\text{Nb}_2\text{O}_5$  catalysts and their photocatalytic for 4-nitrophenol photooxidation in aqueous dispersion, *J. Mater. Sci.* 32 (1997) 6039–6047.
- [19] S. Supothina, P. Seeharaj, S. Yoriya, M. Sriyudthsak, Synthesis of tungsten oxide nanoparticles by acid precipitation method, *Ceram. Int.* 33 (2007) 931–936.
- [20] T. Martinez, A. Bertron, E. Ringot, G. Escadeillas, Degradation of NO using photocatalytic coatings applied to different substrates, *Build. Environ.* 46 (2011) 1808–1816.
- [21] G.R. Bamwenda, H. Arakawa, The photoinduced evolution of  $\text{O}_2$  and  $\text{H}_2$  from a  $\text{WO}_3$  aqueous suspension in the presence of  $\text{Ce}^{4+}/\text{Ce}^{3+}$ , *Sol. Energy Mater. Sol. Cells* 70 (2001) 1–14.